

UNIVERSITY OF CALIFORNIA

Santa Barbara

Point-to-Point Control near Heteroclinic Orbits: Plant and  
Controller Optimality Conditions

A thesis submitted in partial satisfaction of the  
requirements for the degree of Master of Science  
in Mechanical Engineering

by

Brian Paden

Committee in charge:

Professor Jeff Moehlis, Chair

Professor Bassam Bamieh

Professor Francesco Bullo

June 2013

The thesis of Brian Paden is approved.

---

Professor Bassam Bamieh

---

Professor Francesco Bullo

---

Professor Jeff Moehlis, Committee Chair

May 2013

## Acknowledgments

I would first like to thank Professor Jeff Moehlis for his help and guidance. His advising was invaluable in preparing this thesis as well as in many aspects of my graduate studies. I would also like to acknowledge all of the faculty in the Department of Mechanical Engineering at UCSB for their excellent teaching.

# Abstract

## Point-to-Point Control near Heteroclinic Orbits: Plant and Controller Optimality Conditions

by

Brian Paden

In this thesis we consider the simultaneous optimization of the controller and plant in a one degree-of-freedom system. In particular we are interested in optimal trajectories between fixed points connected by heteroclinic orbits. We find that designing the plant dynamics to have a heteroclinic connection between target states enables low energy transfer between the states. We use a nested optimization strategy to find the optimal plant dynamics and control effort to transition between states. Additionally, we uncover plant optimality conditions which reduce the complexity of the optimization.

# Contents

<b>1</b>	<b>Introduction</b>	<b>1</b>
<b>2</b>	<b>Heteroclinic Orbits and Energy Efficient Motion Control</b>	<b>3</b>
<b>3</b>	<b>Problem Statement</b>	<b>6</b>
3.1	Conditions of an Admissible System Design . . . . .	7
3.2	Existence of a control with bounded cost . . . . .	8
<b>4</b>	<b>Optimality Conditions for the Control</b>	<b>9</b>
4.1	Continuous dependence on parameters . . . . .	10
4.2	Properties of the solution to (4.5) for small $\alpha$ . . . . .	11
<b>5</b>	<b>Optimality Conditions for the Plant</b>	<b>13</b>
<b>6</b>	<b>Applications to Mechatronics</b>	<b>17</b>
6.1	Description of the device . . . . .	17
6.2	Equations of motion . . . . .	19
6.3	Control objective . . . . .	23
6.4	Applying the plant optimality conditions . . . . .	23
6.5	A hypothesis . . . . .	25
6.6	Numerical validation of optimal plant design . . . . .	26
6.7	Numerical results . . . . .	28
<b>7</b>	<b>Discussion and Conclusions</b>	<b>32</b>

## List of Figures

2.1	A simple pendulum with a control torque $u(t)$ swinging the pendulum through a rotation of $2\pi$ between unstable equilibria. . . . .	4
2.2	As $\omega_n$ is varied from the values 0, 0.1, 0.3, 0.5, and 1, one can see in (a) the significant reduction in control effort required for the point to point control. The effect on the state trajectory can be seen in (b). . . . .	6
4.1	Minimum energy trajectories for the fixed time pendulum swing up problem. Solutions are computed for $\omega_n^2$ equal to 0.5, 1, 2, and 4. . . . .	12
6.1	An actuator provides the control force to the system while the cam assembly provides the desired nonlinear dynamics. The center two pivots allow the cam follower to track the cam profile while the outer pivots are linked together (not shown) so the distance between the two is fixed. This design feature prevents radial loads from being transmitted to the drive shaft as a result of small differences in spring rate of the two springs. . . . .	18
6.2	The cam profile, $p(s)$ , and the cam follower path, $H(x_1)$ , are distinguished. By varying the contact angle a component of the contact force is projected in the direction of motion $x_1$ . . . . .	20
6.3	An illustration of the limitations on the cam follower path's curvature. As the cam follower passes over a corner, it attains its minimum curvature. Alternatively, as the cam profile's curvature becomes equal to the curvature of the cam follower, the curvature of the cam follower's path becomes unbounded. . . . .	22
6.4	An example of $\kappa(x)$ in the approximation to the design space where the resulting plant would be admissible and satisfy the necessary conditions given in Lemma 1 and Theorem 5. . . . .	27
6.5	Plot of optimal cam curvature satisfying the KKT conditions. $a$ indicates the location $x = \frac{x_f - x_0}{2} - \frac{\varepsilon(x_f - x_0)}{2(r + 2\varepsilon)}$ and $b$ indicates the location $x = \frac{x_f - x_0}{2} + \frac{\varepsilon(x_f - x_0)}{2(r + 2\varepsilon)}$ . . . . .	30
6.6	An illustration of the optimal cam follower path. The dotted and dashed line show the cam follower path at maximum and minimum curvature respectively. Arrow (a) indicates the cam profile for the corresponding cam follower path. Arrow (b) indicates the system configuration determined by the center of the cam follower, while arrow (c) indicates the contact location of the cam follower with the cam surface for the illustrated configuration. . . . .	31
6.7	The optimal state trajectory (in bold) is plotted over the level sets of the Hamiltonian (mechanical energy) of the optimal plant design to demonstrate how the optimal trajectory tends to follow the natural motion of the plant. . . . .	32

# 1 Introduction

The traditional practice for designing mechatronic systems is to first design the structure, sensors, and actuators, followed by the design of the controller. This design approach has been referred to as the sequential or single pass strategy [14, 13, 3]. Numerous mathematical and computational tools exist for optimizing these two subsystems independently [1, 11]. However, it was proven in [3] that this approach does not necessarily satisfy the system level optimality conditions. To solve the problem of finding the optimal plant and controller, several strategies have been proposed. These are classified as iterative, nested, and simultaneous optimization strategies [3]. The benefit of these strategies is that they yield an optimal system design, and they have subsequently found their way into a number of engineering applications [4, 12, 9, 2].

In this thesis, we will consider the energy cost of holding the state of the system at an initial stationary configuration up to an initial time at which the control will transfer the state to a final stationary configuration where it will remain indefinitely. The problem is to choose the best plant dynamics within an admissible design space so that the energy cost associated with the control task is minimized. If it is possible to design the plant so that the initial and final states are connected by a heteroclinic orbit [5] then without external disturbances there will be no cost associated with holding the system at the initial and final states. Then, with little effort from the controller, the plant dynamics will help to carry the state between equilibria in finite time.

Such a system has several useful applications, one of which is the electronic control of internal combustion engine valves. Electronically actuated engine valves

would enable the phase of the valve opening and closing events to be varied in order to improve engine performance. Implementation of electronically controlled engine valves has already been tested and has been shown to significantly reduce emissions and increase fuel economy and power [6]. The drawback to many of these systems is that they require prohibitive amounts of energy to operate, which counteracts the improvements in efficiency. This has inspired the use of additional mechanisms coupled to the linear actuator that are intended to reduce the power required to drive the engine valve [10]. The goal of this thesis is to present optimality conditions useful for optimizing electromechanical systems for high efficiency point-to-point control.

In Section 2 we consider the optimal open loop control to swing around an inverted pendulum to better understand the gains of actuating a system between the fixed points of a heteroclinic orbit. Section 3 extends the problem to finding the optimal plant dynamics as well as the optimal control. For computing the system-wide optimization we will use the nested optimization strategy. An inner loop will optimize the control for each plant design we consider using optimal control theory. The inner loop optimization is covered in Section 4. The outer loop numerically optimizes the plant design by considering the optimal control for each fixed plant design we consider. To reduce the computational expense of this optimization we will derive optimality conditions of the optimal plant design. These conditions are derived in Section 5. In Section 6, a versatile mechatronic system is introduced that we optimize by applying the methods outlined. Conclusions and a discussion of future research are given in Section 7.

## 2 Heteroclinic Orbits and Energy Efficient Motion Control

Here we will study the benefits of choosing a plant potential that connects two target configurations with a heteroclinic orbit. Consider the problem of finding the minimum energy control torque  $u(t)$  to swing around an inverted pendulum of unit mass. The dynamics will be given by

$$\dot{x}_1 = x_2, \quad \dot{x}_2 = -\omega_n^2 \sin(x_1) + u(t). \quad (2.1)$$

We want to solve for the minimum energy control effort connecting the initial state,  $(x_1(t_0), x_2(t_0)) = (-\pi, 0)$ , to the final state,  $(x_1(t_f), x_2(t_f)) = (\pi, 0)$ . We consider the state to be in  $\mathbb{R}^2$  as opposed to  $\mathbb{R} \times S^1$ .

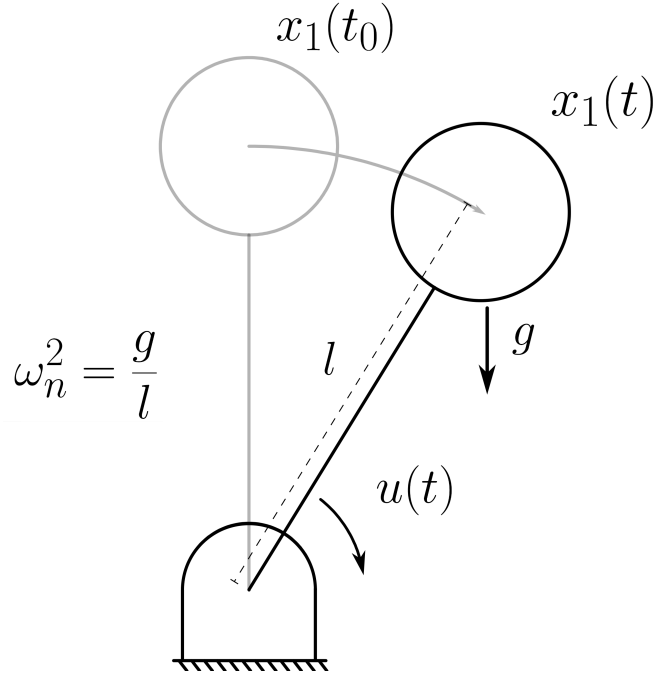


Figure 2.1: A simple pendulum with a control torque  $u(t)$  swinging the pendulum through a rotation of  $2\pi$  between unstable equilibria.

We can make direct use of Pontryagin's minimum principle [1] to represent necessary conditions of an optimal control in the form of a boundary value problem (BVP). The cost functional we impose to find a minimum energy control is

$$J[u] = \int_{t_0}^{t_f} [u(t)]^2 dt. \quad (2.2)$$

The Hamiltonian for this system and cost functional is

$$H(x_1, x_2, u, p_1, p_2) = u^2 + \left\langle \begin{pmatrix} p_1 \\ p_2 \end{pmatrix}, \begin{pmatrix} x_2 \\ -\omega_n^2 \sin(x_1) + u \end{pmatrix} \right\rangle, \quad (2.3)$$

where  $p_1$  and  $p_2$  are the co-state variables. Then, using the canonical equations

we derive the necessary conditions of the optimal control:

$$\frac{\partial H}{\partial u} = 0, \quad \frac{\partial H}{\partial p_1} = \dot{x}_1, \quad \frac{\partial H}{\partial p_2} = \dot{x}_2, \quad \frac{\partial H}{\partial x_1} = -\dot{p}_1, \quad \frac{\partial H}{\partial x_2} = -\dot{p}_2, \quad (2.4)$$

which yields:

$$\begin{aligned} \dot{x}_1 &= x_2, & \dot{x}_2 &= -\omega_n^2 \sin(x_1) - p_2/2, \\ \dot{p}_1 &= p_2 \omega_n^2 \cos(x_1), & \dot{p}_2 &= -p_1, & u &= -p_2/2, \end{aligned} \quad (2.5)$$

$$(x_1(t_0), x_2(t_0)) = (-\pi, 0), \quad (x_1(t_f), x_2(t_f)) = (\pi, 0).$$

The case when  $\omega_n = 0$  will be considered as a basis of comparison with various values of  $\omega_n$ .

The shooting method in conjunction with the Nelder-Mead simplex method [7] was implemented to solve equation (2.5) for  $t_0 = 0$  and  $t_f = 10$ .  $\omega_n$  was varied in equation (2.5) to demonstrate the benefit of the heteroclinic orbit introduced by the pendulum dynamics. Figure 2.2 illustrates the significant reduction in control effort as  $\omega_n$  is increased.

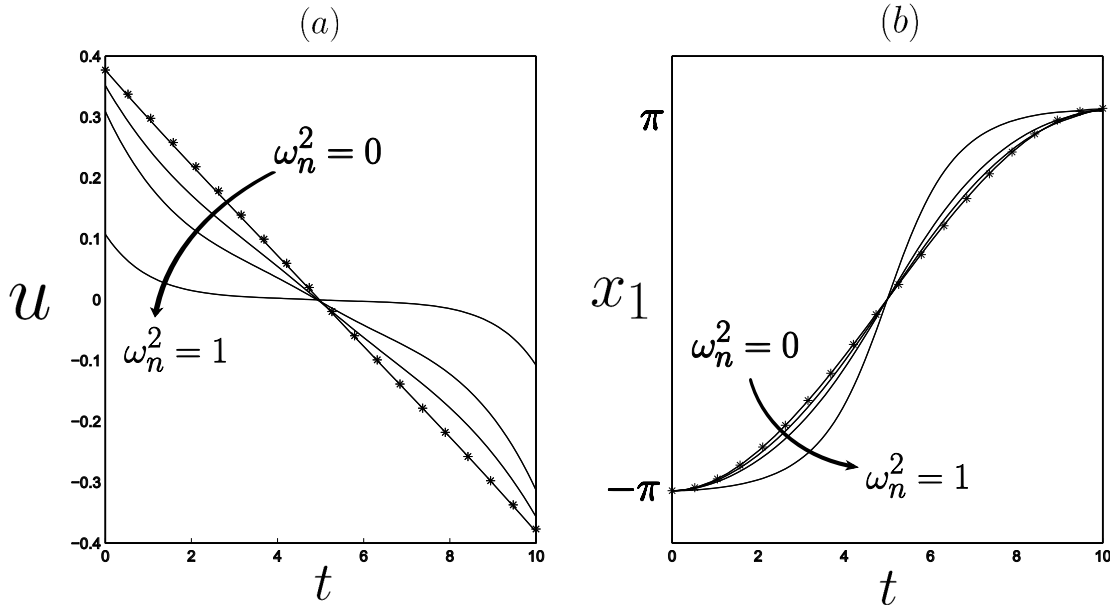


Figure 2.2: As  $\omega_n$  is varied from the values 0, 0.1, 0.3, 0.5, and 1, one can see in (a) the significant reduction in control effort required for the point to point control. The effect on the state trajectory can be seen in (b).

### 3 Problem Statement

It is clear that introducing a heteroclinic orbit connecting the target configurations for point to point control reduces the energy cost. With this in mind we now consider the simultaneous optimization of the plant and control.

Consider a system of the form

$$\dot{x}_1 = x_2, \quad \dot{x}_2 = \alpha f(x_1) + u(t), \quad (3.1)$$

with  $\alpha > 0$ . A trajectory produced under the influence of  $\alpha f$  and  $u$  will be

considered admissible if it satisfies (3.2):

$$(x_1(t), x_2(t)) = (x_0, 0) \quad \forall t \in [-\infty, t_0], \tag{3.2}$$

$$(x_1(t), x_2(t)) = (x_f, 0) \quad \forall t \in [t_f, \infty].$$

That is, up to time  $t_0$  the state is held at  $(x_0, 0)$ . The control then transfers the state to  $(x_f, 0)$ , where it must arrive by time  $t_f$ . The state must then remain there indefinitely. We will assume without loss of generality that  $x_0 < x_f$ .

### 3.1 Conditions of an Admissible System Design

Here we define the conditions on the control effort,  $u$ , and the plant dynamics,  $f$ , for an admissible system design. We require that the control effort remain bounded and piecewise continuous;  $\Omega$  will denote the set of admissible controls for which these conditions hold. We require  $f$  to satisfy the constraint (3.3) almost everywhere.

$$g(x) \leq \psi(f(x), f'(x), \dots, f^{(n)}(x)) \leq h(x). \tag{3.3}$$

We say almost everywhere because it will only be required that  $f$  be  $n$  times piecewise continuously differentiable, and  $f'$  be Lipschitz continuous ( $n$  must be greater than 1). The functions  $g$  and  $h$  are continuous real valued functions defined on  $[x_0, x_f]$ . The function  $\psi$  is a continuous vector valued function from  $\mathbb{R}^n$  into  $\mathbb{R}$ . The functions  $g$ ,  $h$  and  $\psi$ , as well as the dimension,  $n$ , of  $\psi$  will be determined by the particular application. Assume  $g(x) \leq h(x) \forall x \in [x_0, x_f]$

so that there may exist an admissible  $f$ . For each  $x \in [x_0, x_f]$ ,  $\psi$  is evaluated at  $(f(x), f'(x), \dots, f^{(n)}(x))$  and must satisfy (3.3). The construction of this constraint is intended to capture a broad range of design constraints one might encounter. For example, in mechanical systems there may be constraints on the rate at which  $f$  changes in order to control dynamic loads or to satisfy geometric constraints. *We will define the set  $F$  as the set of all  $f$  satisfying (3.3) with Lipschitz continuous first derivative.*

*An ordered pair  $(f, u) \in F \times \Omega$  will be referred to as a system design, and a system design will be called admissible if a solution to equation (3.1) passing through  $(x_0, 0)$  at  $t_0$  is an admissible state trajectory. The cost associated with an admissible system design is*

$$J[u, f] = \int_{-\infty}^{\infty} [u(t)]^2 dt. \quad (3.4)$$

*An admissible system design  $(f^*, u^*)$  is optimal if  $J[u^*, f^*] \leq J[u, f]$  for all admissible system designs. The problem is to find the optimal system design.*

### 3.2 Existence of a control with bounded cost

The existence of a bounded cost control effort when  $f(x_0) = 0$  and  $f(x_f) = 0$  is easily proven by considering the following control effort. Let  $u(t) = -\alpha f(x_1(t)) - 6(2t - t_0 - t_f)(x_0 - x_f)/(t_0 - t_f)^3$  on  $[t_0, t_f]$  and zero everywhere else. This gives rise to an admissible state trajectory. In particular, the resulting cubic  $x_1$  trajectory satisfies (3.2). This control is constructed by first calculating the admissible cubic  $x_1$  trajectory. We evaluate  $\alpha f(x_1(t))$  along this trajectory and choose the first

term of  $u(t)$  to feedback linearize the system. For the second term of  $u$  we add  $\ddot{x}_1$  for the cubic trajectory to  $u$ . It is easy to see that the control will give rise to the desired trajectory.  $f(x_1)$  is bounded on  $[x_0, x_f]$  which guarantees that  $u(t)$  is bounded on  $[t_0, t_f]$ . Since  $f(x_0) = 0$  and  $f(x_f) = 0$ ,  $u(t) = 0$  for  $t \notin [t_0, t_f]$ . Then  $u(t)$  is bounded, continuous, and is only nonzero on a closed interval. Thus, (3.4) is bounded. By this construction we can always find a control effort with bounded cost if  $f(x_0) = 0$  and  $f(x_f) = 0$ .

## 4 Optimality Conditions for the Control

Recall that in Section 2 we implemented classical optimal control techniques to compute the minimum energy trajectory between the fixed points of a heteroclinic orbit. Here we will apply the same techniques to (3.1) to represent the necessary conditions of an optimal  $u$  on  $[t_0, t_f]$  for a fixed  $\alpha f$  in the form of a BVP. This will allow us to find the optimal control for a fixed plant  $\alpha f$ . This approach will be used to run the inner loop of the system optimization.

To be clear, we are considering the dynamical system

$$\dot{x}_1 = x_2, \quad \dot{x}_2 = \alpha f(x_1) + u(t). \quad (4.1)$$

with  $\alpha > 0$  and the cost functional

$$J[u] = \int_{t_0}^{t_f} [u(t)]^2 dt, \quad (4.2)$$

and boundary conditions

$$(x_1(t_0), x_2(t_f)) = (x_0, 0), \quad (x_1(t_f), x_2(t_f)) = (x_f, 0). \quad (4.3)$$

The Hamiltonian for this system is then

$$H(x_1, x_2, u, p_1, p_2) = u^2 + \left\langle \begin{pmatrix} p_1 \\ p_2 \end{pmatrix}, \begin{pmatrix} x_2 \\ \alpha f(x_1) + u \end{pmatrix} \right\rangle. \quad (4.4)$$

From (2.4) we arrive at necessary conditions on an optimal  $u$  in the form of a BVP:

$$\begin{aligned} \dot{x}_1 &= x_2, & \dot{x}_2 &= \alpha f(x_1) - p_2/2, \\ \dot{p}_1 &= -\alpha p_2 f'(x_1), & \dot{p}_2 &= -p_1, & u &= -p_2/2, \end{aligned} \quad (4.5)$$

$$(x_1(t_0), x_2(t_0)) = (x_0, 0), \quad (x_1(t_f), x_2(t_f)) = (x_f, 0).$$

## 4.1 Continuous dependence on parameters

It is shown in [8] that if there is a unique optimal control at a particular parameter value  $\alpha_0$ , then the optimal control and state trajectory are differentiable with respect to  $\alpha$  at  $\alpha_0$ . Thus, they also depend continuously on  $\alpha$  at  $\alpha_0$ . Then given  $\varepsilon > 0$  there exists  $\alpha$  sufficiently close to  $\alpha_0$  such that:

$$\|z(t, \alpha) - z(t, \alpha_0)\| < \varepsilon \quad \forall t \in [t_0, t_f], \quad (4.6)$$

where  $z = (x_1, x_2, p_1, p_2)^T$ .

## 4.2 Properties of the solution to (4.5) for small $\alpha$

We now will point out an important property of the solution to (4.5). Let  $\alpha = 0$ . The solution,  $(\tilde{x}_1, \tilde{x}_2, \tilde{p}_1, \tilde{p}_2)$ , to the system when  $\alpha = 0$  is easily solved and found to be unique since (4.5) becomes linear. In particular we are interested in  $\tilde{x}_2$ :

$$\tilde{x}_2(t) = \frac{6(t-t_0)(t_f-t)(x_f-x_0)}{(t_f-t_0)^3}. \quad (4.7)$$

From (4.7) we see that  $\tilde{x}_2(t) > 0$  on  $(t_0, t_f)$ . From Section 4.1, solutions depend continuously on  $\alpha$  at  $\alpha = 0$ . Then for any  $\varepsilon > 0$  there exists a sufficiently small  $|\alpha| > 0$  such that

$$|x_2(t) - \tilde{x}_2(t)| < \varepsilon \forall t \in [t_0, t_f], \quad (4.8)$$

where  $x_2(t)$  satisfies (4.5). It follows that for  $\alpha$  sufficiently small,  $x_2(t) > 0 \forall t \in (t_0, t_f)$ .

To prove the claim, suppose that there is no such  $\alpha > 0$ . Then for all  $\alpha > 0$ ,  $\exists t^* \in (t_0, t_f)$  such that  $x_2(t^*) \leq 0$ . From (4.7),  $\tilde{x}_2(t^*) > 0$ . Thus, for some  $\varepsilon > 0$ ,  $\tilde{x}_2(t^*) - x_2(t^*) = \varepsilon$ . This is a contradiction of (4.6). *For the remainder of the thesis we consider  $\alpha$  to be small enough for this property to hold.*

Next,  $x_2(t) > 0 \forall t \in (t_0, t_f)$  and  $\dot{x}_1 = x_2$  implies that  $x_1$  is one-to-one on  $[t_0, t_f]$ . This is also proven by contradiction. Suppose that  $x_1$  is not one-to-one on  $[t_0, t_f]$ . Then there are two distinct points  $\tau_1$  and  $\tau_2$  in  $[t_0, t_f]$  for which  $x_1(\tau_1) = x_1(\tau_2)$  (assume without loss of generality that  $\tau_1 < \tau_2$ ). Since  $x_2$  is

continuous,  $x_1$  is differentiable. So by application of Rolle's Theorem [15] there exists a time  $\tau^* \in (\tau_1, \tau_2) \subseteq (t_0, t_f)$  where  $\dot{x}_1(\tau^*) = 0$ , and thus  $x_2(\tau^*) = 0$ . This is a contradiction of the previous observation that  $x_2(t) > 0 \forall t \in (t_0, t_f)$ .

To demonstrate the monotonicity of the  $x_1$  trajectory solving (4.5), we consider the minimum energy control for (2.5) with initial conditions  $(x_1(t_0), x_2(t_0)) = (0, 0)$  instead of  $(x_1(t_0), x_2(t_0)) = (-\pi, 0)$  (i.e. the minimum energy pendulum swing up problem). This problem is solved numerically using the same scheme as in Section 2. By varying  $\omega_n$  we see that below some critical value, the  $x_1$  trajectory is monotonic. Figure 4.1 shows how the state trajectory exhibits oscillations for larger values of  $\omega_n$ .

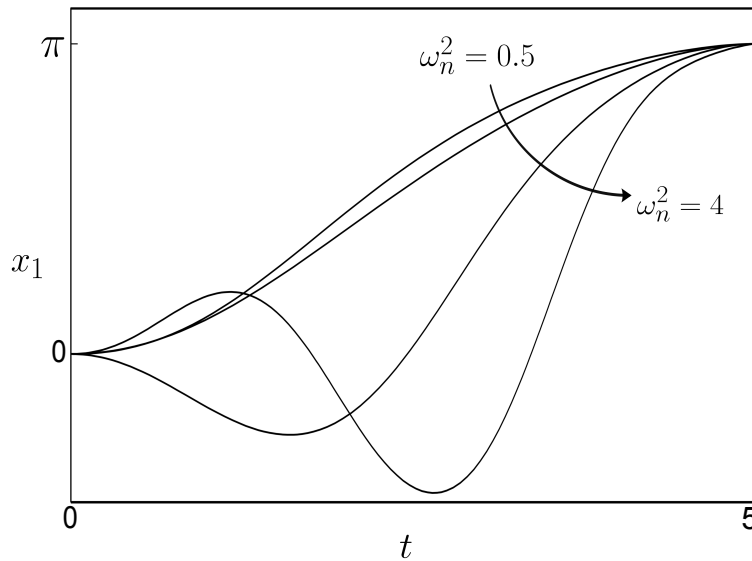


Figure 4.1: Minimum energy trajectories for the fixed time pendulum swing up problem. Solutions are computed for  $\omega_n^2$  equal to 0.5, 1, 2, and 4.

The purpose of this example is to demonstrate that the perturbation parameter ( $\omega_n$  in this case) may be quite large before the optimal  $x_1$  trajectory loses its monotonicity. Additionally, if we refer back to Figure 2.2 for the pendulum swing

around problem, we see that for all values of  $\omega_n$  considered,  $x_1$  was monotonic.

## 5 Optimality Conditions for the Plant

With a procedure to optimize the inner loop (control) of the nested optimization we now consider the optimization of the plant. For each plant design considered we must numerically solve a BVP to find the optimal control effort for that plant design. Thus evaluating the cost of a particular plant design is computationally expensive. For this reason the plant dynamics must be optimized efficiently. Theorem 5 will provide optimality conditions for an optimal plant design. The following Lemmas are needed for the proof of Theorem 5.

**Lemma 1.** *If a pair  $(f^*, u^*)$  is optimal, then  $f^*(x_0) = 0$  and  $f^*(x_f) = 0$ ; and if no such plant design is admissible, then all designs have unbounded cost.*

*Proof.* Suppose  $f^*(x_0) \neq 0$  (An analogous argument holds for  $f^*(x_f) \neq 0$ ). Then  $u(t) = -f(x_0) \forall t \in (-\infty, t_0)$  so that the cost (4.7) is unbounded. This is a contradiction since we have already established the existence of a bounded cost solution when there is an admissible design with  $f^*(x_0) = 0$  and  $f^*(x_f) = 0$ .

□

**Lemma 2.** *Suppose  $u^*$  is an optimal control for the system. Then there is no interval  $(\tau_1, \tau_2) \subseteq (t_0, t_f)$  where  $u^*(t) = 0$  for all  $t \in (\tau_1, \tau_2)$ .*

*Proof.* Suppose there exists a time interval  $(\tau_1, \tau_2)$  where  $u^*(t) = 0$  for  $t \in (\tau_1, \tau_2)$ . Then  $\dot{u}^*(t) = 0$  for  $t \in (\tau_1, \tau_2)$  as well. Since  $u^* = -p_2/2$ , then  $p_2(t) = 0$  and  $\dot{p}_2(t) = 0$  for  $t \in (\tau_1, \tau_2)$ . From equation (4.5) it follows that  $p_1(t) = 0$  and  $\dot{p}_1(t) = 0$  for  $t \in (\tau_1, \tau_2)$ , the costates will be zero for all  $t > \tau_1$ . Then the motion of the system for  $t > \tau_1$  is governed by

$$\dot{x}_1 = x_2, \quad \dot{x}_2 = \alpha f(x_1). \quad (5.1)$$

From Lemma 1 and (5.1) the terminal state  $(x_f, 0)$  will be a fixed point of the system. Recall that  $x_1(t)$  is one-to-one on  $[t_0, t_f]$  and  $x(t_f) = x_f$ . So for  $t \in (\tau_1, \tau_2)$ ,  $x_1(t) \neq x_f$ . Then  $x_1(t)$  cannot reach the fixed point at  $x_f$  in finite time. Hence, such a control would lead to an inadmissible trajectory.

□

**Lemma 3.** *If  $u \in \Omega$ ,  $\phi \in C^n(t_0, t_f)$  and  $\langle u, \phi \rangle_{L_2[t_0, t_f]} > 0$ , then for all  $\varepsilon \in \left(\frac{-2\langle u, \phi \rangle}{\|\phi\|^2}, 0\right)$ ,  $\|u + \varepsilon\phi\|_{L_2[t_0, t_f]} < \|u\|_{L_2[t_0, t_f]}$  (If  $\langle u, \phi \rangle < 0$  then the statement is instead true for  $\varepsilon \in \left(0, \frac{-2\langle u, \phi \rangle}{\|\phi\|^2}\right)$ ).*

*Proof.* For brevity the subscript  $L_2[t_0, t_f]$  will be dropped from norms and inner products for the remainder of this calculation.

$$\begin{aligned} \|u + \varepsilon\phi\|^2 &= \langle u + \varepsilon\phi, u + \varepsilon\phi \rangle \\ &= \langle u, u \rangle + 2\langle u, \varepsilon\phi \rangle + \langle \varepsilon\phi, \varepsilon\phi \rangle \end{aligned}$$

$$= \|u\|^2 + 2\varepsilon \langle u, \phi \rangle + \varepsilon^2 \|\phi\|^2.$$

Notice that the right hand side of the equation is quadratic in  $\varepsilon$ . The quadratic equation  $0 = 2\varepsilon \langle u, \phi \rangle + \varepsilon^2 \|\phi\|^2$  is convex with zeros at  $\varepsilon = \frac{-2\langle u, \phi \rangle}{\|\phi\|^2}$  and  $\varepsilon = 0$ . Without loss of generality, assume that  $\langle u, \phi \rangle > 0$ . Then  $0 > 2\varepsilon \langle u, \phi \rangle + \varepsilon^2 \|\phi\|^2$  for all  $\varepsilon$  greater than  $\frac{-2\langle u, \phi \rangle}{\|\phi\|^2}$  and less than 0. Then we conclude that

$$\|u + \varepsilon\phi\|^2 < \|u\|^2 \quad \forall \varepsilon \in \left( \frac{-2\langle u, \phi \rangle}{\|\phi\|^2}, 0 \right).$$

□

**Definition 4.** The norm  $\|\cdot\|_{\dagger}$  acts on the function space  $C^m[x_0, x_f]$  and is defined:

$$\|f\|_{\dagger} \equiv \max \left\{ \max \{|f(x)|\}, \dots, \max \{|f^{(n)}(x)|\} \right\} \quad \forall x \in [x_0, x_f]$$

**Theorem 5.** *If  $(f^*, u^*)$  are the optimal design, then for all  $x \in [x_0, x_f]$ , the constraint (3.3) is active.*

*Proof.* The proof is by contradiction. Suppose that  $(f^*, u^*)$  are the optimal design, and that at some point  $p \in [x_0, x_f]$ , (3.3) is not active. Then by the continuity of  $\psi$  there exists a closed interval  $[a, b]$  containing the point  $p$  such that,  $h(x_1) < \psi(f(x_1), f'(x_1), \dots, f^n(x_1)) < g(x_1) \forall x_1 \in [a, b]$ . Again making use of the continuity of  $\psi$  there exists a  $\delta > 0$  such that for all  $x_1 \in [a, b]$ ,  $h(x_1) < \psi(f(x_1) \pm \varepsilon, f'(x_1) \pm \varepsilon, \dots, f^n(x_1) \pm \varepsilon) < g(x_1)$  (by  $\pm \varepsilon$  we mean the ball in  $\mathbb{R}^n$  of radius  $\varepsilon$ , centered

at  $(f(x_1), f'(x_1), \dots, f^n(x_1))$  in the  $\infty$ -norm). Consider any  $\phi \in C^n[a, b]$  where  $\phi(x) = 0$  for  $x_1 \notin (a, b)$ . Then for  $\delta$  satisfying  $0 < \delta \leq \varepsilon / \|\phi\|_{\dagger}$ ,  $h(x) < C(f(x_1) \pm \delta\phi(x_1), f'(x_1) \pm \delta\phi'(x_1), \dots, f^n(x_1) \pm \delta\phi^n(x_1)) < g(x_1) \forall x_1 \in [a, b]$ .

Now suppose we wanted to maintain the same trajectory as in the optimal design with the plant design perturbed by  $\delta\phi$ . Then the control effort must be modified to account for the change in the plant design. That is,

$$\alpha f^*(x_1^*(t)) + u^*(t) = \alpha f^*(x_1^*(t)) + \delta\alpha\phi(x_1^*(t)) + u^*(t) + \eta(t),$$

$$\Rightarrow \eta(t) = -\delta\alpha\phi(x_1^*(t)).$$

Since  $x_1(t)$  is one-to-one on  $[t_0, t_f]$  it is not difficult to construct  $\phi$  so that  $\langle u^*(t), \alpha\phi(x_1^*(t)) \rangle_{L_2(t_0, t_f)} \neq 0$ . For example, one could choose  $\phi$  to satisfy  $\text{sgn}(\phi(x_1^*(t))) = \text{sgn}(u^*(t))$  while  $x_1(t)$  is on the interval  $(a, b)$ . Define  $t_a$  and  $t_b$  by  $x_1^*(t_a) = a$ ,  $x_1^*(t_b) = b$ . From Lemma 2  $u(t) \neq 0$  for all  $t$  on  $[t_a, t_b]$ . It then follows from the construction of  $\phi$  and the properties of  $u$  that  $u^*(t)\phi(x_1^*(t)) > 0$  on  $[t_a, t_b]$  which implies  $\langle u^*(t), \alpha\phi(x_1^*(t)) \rangle_{L_2(t_0, t_f)} > 0$ . Now applying Lemma 3 we know that we can find  $\varepsilon \leq \delta / \|\phi\|_{\dagger}$  such that  $\|u^* - \varepsilon\alpha\phi\|_{L_2(t_0, t_f)} < \|u^*\|_{L_2(t_0, t_f)}$  and thus,  $\|u^* + \eta\|_{L_2(t_0, t_f)} < \|u^*\|_{L_2(t_0, t_f)}$ . Then there exists a perturbation from our optimal plant design with a lower cost control. This is a contradiction, and hence the constraints on  $f$  must always be active. □

It immediately follows from the proof of Theorem 5 that if the plant has no constraints other than a Lipschitz continuous first derivative, then an optimal system design does not exist.

The optimality conditions proven in Theorem 5 reduce the computational expense of optimizing the plant design by restricting the optimization to a subset of  $F$ . *The subset of the plant design space  $F$  where the optimality conditions are satisfied will be denoted  $\tilde{F}$ .*

## 6 Applications to Mechatronics

Here we describe a simple linear actuation system whose dynamics can be chosen from a large design space. This example illustrates the ideas presented in this thesis.

### 6.1 Description of the device

Consider the mechatronic system shown in Figure 6.1 for linear actuation of a mass between two configurations.

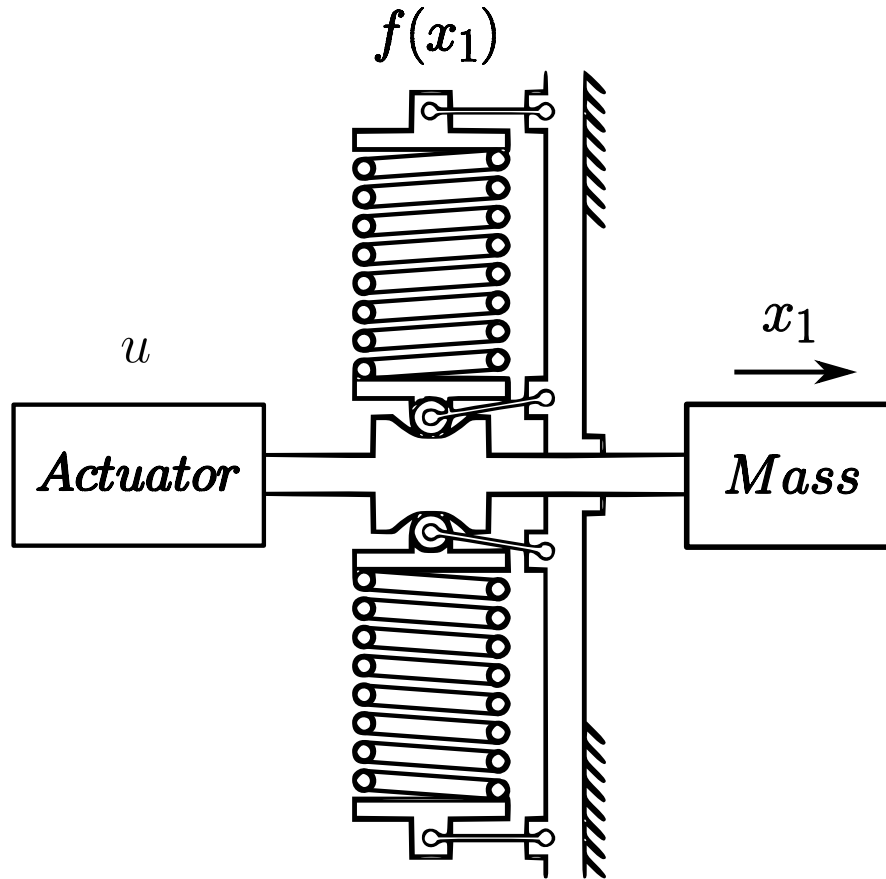


Figure 6.1: An actuator provides the control force to the system while the cam assembly provides the desired nonlinear dynamics. The center two pivots allow the cam follower to track the cam profile while the outer pivots are linked together (not shown) so the distance between the two is fixed. This design feature prevents radial loads from being transmitted to the drive shaft as a result of small differences in spring rate of the two springs.

A conventional linear actuator provides a control force directly to the mass through a rigid connection. Coupled in parallel to the actuator is a cam and spring mechanism intended to project a force in the direction of motion that assists the control by appropriate design of the cam. The cam is fixed to the shaft that drives the mass. The cam followers are preloaded against the cam by coil springs and their motion is constrained so that they can only move normal to

the motion of the mass. We will assume the cam followers are frictionless and of negligible mass.

## 6.2 Equations of motion

The displacement  $x_1$  shown in Figure 6.1 measures the configuration of the system. The state of the system can be described by the ordered pair  $(x_1, x_2)$  where  $x_1$  gives the configuration and  $x_2$  the velocity. It will be assumed that the mass of the payload is much larger than the mass of any other moving parts. The mechanism provides a force  $f(x_1)$  on the mass that depends on the configuration. The linear actuator provides the control force  $u(t)$  on the mass. The resulting equations of motion are then

$$\dot{x}_1 = x_2, \quad \dot{x}_2 = f(x_1) + u(t). \quad (6.1)$$

Now we will calculate how the choice of cam will affect the dynamics and derive the design constraints. Let  $k$  be the combined spring constant of the springs providing force to the cam followers. Let  $H(x_1)$  be the displacement of the center of each cam follower away from the rigid shaft with respect to the configuration. Note that the mechanism is symmetric, so each of the cam followers will be of equal distance from the shaft at any particular configuration. Let  $H(x_0) = 0$  (recall that  $x_0$  is one of the target configurations described in Section 3). Let  $r$  be the radius of the cam follower, and let  $p(s)$  describe the cam profile with respect to the contact location  $s$ . By examining Figure 6.2 it is clear that  $s$  is not always equal to  $x_1$ . However, it is not difficult to compute  $p(s)$  given  $H(x_1)$  and vice versa, so it is sufficient to design the mechanism in terms of  $H(x_1)$  and compute

$p(s)$  for the manufacture of the cams.

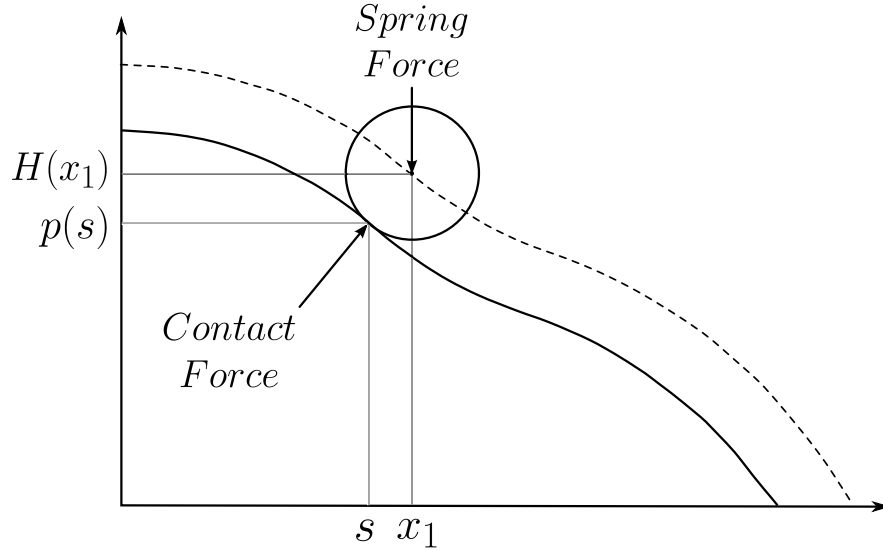


Figure 6.2: The cam profile,  $p(s)$ , and the cam follower path,  $H(x_1)$ , are distinguished. By varying the contact angle a component of the contact force is projected in the direction of motion  $x_1$ .

We can now compute the force that this setup produces in the direction of motion. A simple calculation yields  $f(x_1) = k(H(x_1) + \delta_0)H'(x_1)$ , where  $\delta_0$  is the deflection of the spring at the initial configuration. We will assume that  $\delta_0 \gg H(x_1)$  throughout the interval  $[x_0, x_1]$  so that  $k(H(x_1) + \delta_0)$  is approximately a constant  $F_0$ :

$$f(x_1) = F_0 H'(x_1). \quad (6.2)$$

The results are unchanged without this assumption, but the calculations become tedious. Note that the curvature of the cam follower path is given by

$$\kappa(x_1) = H''(x_1) / \left(1 + [H'(x_1)]^2\right)^{3/2}. \quad (6.3)$$

In reference to Figure 6.3, we see that the minimum curvature of the path taken by

the cam follower is  $-1/r$  at a corner in the cam profile. The maximum curvature of  $\infty$  takes place as the curvature of the cam equals the curvature of the follower. To control impact and Hertzian contact stress the constraints are modified by adding a tolerance,  $\varepsilon > 0$ . The constraint on curvature is then

$$-1/(r + \varepsilon) \leq \kappa(x_1) \leq 1/\varepsilon. \quad (6.4)$$

We can now express the constraint on the the curvature of the cam follower path in terms of the force projected in the direction of motion. Combining equation (6.3) and equation (6.4), the constraint on curvature in terms of the cam follower path is

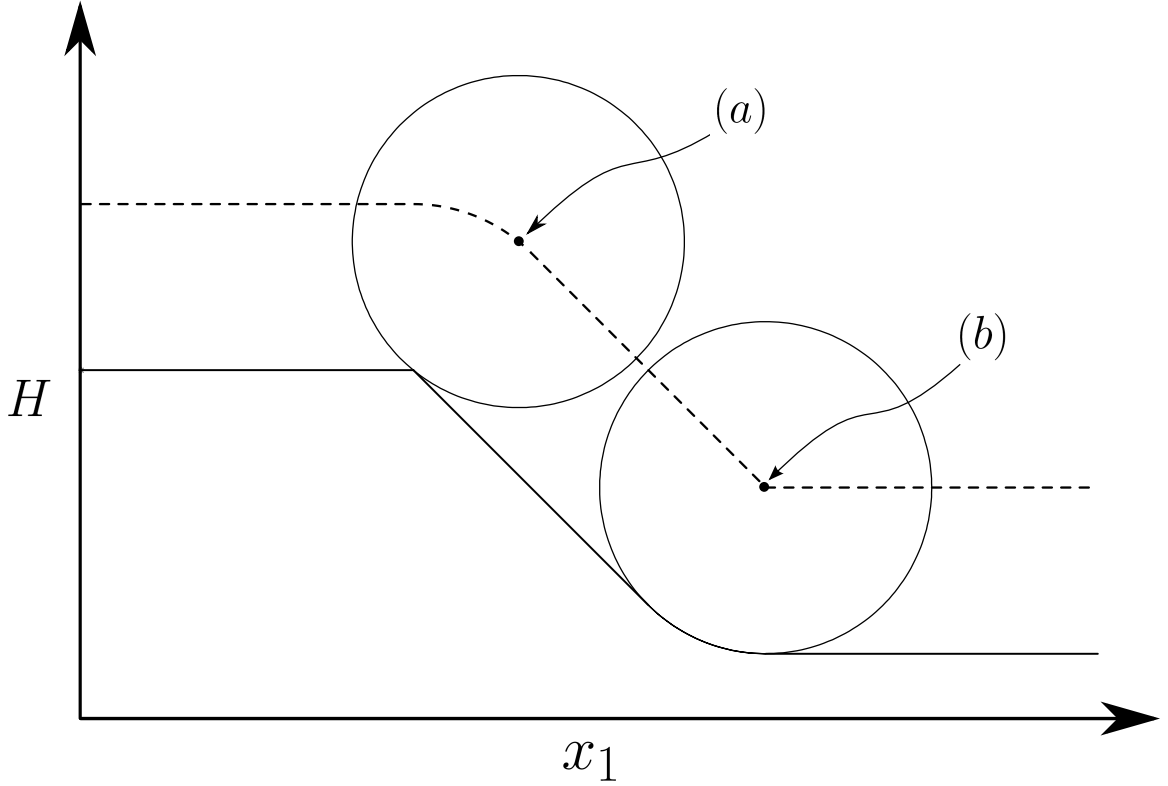


Figure 6.3: An illustration of the limitations on the cam follower path's curvature. As the cam follower passes over a corner, it attains its minimum curvature. Alternatively, as the cam profile's curvature becomes equal to the curvature of the cam follower, the curvature of the cam follower's path becomes unbounded.

$$-\frac{1}{r + \varepsilon} \leq \frac{H''(x_1)}{\left(1 + [H'(x_1)]^2\right)^{3/2}} \leq \frac{1}{\varepsilon}. \quad (6.5)$$

Substitution of equation (6.2) yields

$$-\frac{F_0}{r + \varepsilon} \leq \frac{f'(x_1)}{\left(1 + \left(\frac{f(x_1)}{F_0}\right)^2\right)^{3/2}} \leq \frac{F_0}{\varepsilon}. \quad (6.6)$$

Observe that this constraint takes the form of equation (3.3). Additionally, to apply the results of the previous section to this problem, for  $f(x_1)$  satisfying (6.6) to be an admissible plant design we also require that  $f'(x_1)$  be Lipschitz. Without

this restriction,  $H(x_1)$  could be chosen to have fixed curvature (think of a circular arc). This would be admissible but  $f(x_1)$  could grow unbounded on the interval  $[x_0, x_f]$ . This would lead to unbounded contact stress between the cam surface and cam follower. Requiring Lipschitz continuity eliminates this possibility.

### 6.3 Control objective

The control objective is to maintain the state  $(x_1, x_2) = (x_0, 0)$  on  $(-\infty, t_0)$ . Then on  $[t_0, t_f]$  the control must transfer the state to  $(x_1, x_2) = (x_f, 0)$ . The control then holds the system at  $(x_f, 0)$  on  $(t_f, \infty)$ . The goal is to design  $f(x_1)$  and  $u(t)$  subject to the constraints so that this task is completed while minimizing the energy cost.

### 6.4 Applying the plant optimality conditions

The following calculation uses Lemma 1 to find a condition on the curvature of the cam follower path:

$$\int_{x_0}^{x_f} \frac{H''(x_1)}{\left(1 + [H'(x_1)]^2\right)^{3/2}} dx_1 = \frac{H'(x_f)}{\sqrt{1 + [H'(x_f)]^2}} - \frac{H'(x_0)}{\sqrt{1 + [H'(x_0)]^2}}. \quad (6.7)$$

Making a substitution from (6.2) we have

$$\int_{x_0}^{x_f} \frac{H''(x_1)}{\left(1 + [H'(x_1)]^2\right)^{3/2}} dx_1 = \frac{f(x_f)/F_0}{\sqrt{1 + [f(x_f)/F_0]^2}} - \frac{f(x_0)/F_0}{\sqrt{1 + [f(x_0)/F_0]^2}}. \quad (6.8)$$

Then applying Lemma 1 we have

$$\int_{x_0}^{x_f} \frac{H''(x_1)}{(1 + H'(x_1)^2)^{3/2}} dx_1 = 0. \quad (6.9)$$

This is a useful constraint to place on the design space.

Next, Theorem 5 with (6.6) implies

$$\frac{f'(x_1)}{\sqrt{\left(1 + \left(\frac{f(x_1)}{F_0}\right)^2\right)^3}} = -\frac{F_0}{r + \varepsilon} \quad \text{or} \quad \frac{f'(x_1)}{\sqrt{\left(1 + \left(\frac{f(x_1)}{F_0}\right)^2\right)^3}} = \frac{F_0}{\varepsilon} \quad \forall x \in [x_0, x_f]. \quad (6.10)$$

An equivalent way to express this condition is to express it in terms of the curvature of the cam follower path.

$$\kappa(x) = -\frac{1}{r + \varepsilon} \quad \text{or} \quad \kappa(x) = \frac{1}{\varepsilon} \quad \forall x \in [x_0, x_f]. \quad (6.11)$$

Now since  $\kappa(x)$  is limited to two values for this problem, (6.9) can then be written in the form

$$\int_{x_0}^{x_f} \kappa(x) dx = a \left(\frac{1}{\varepsilon}\right) - b \left(\frac{1}{\varepsilon + r}\right) = 0, \quad (6.12)$$

where  $a$  and  $b$  describe the total length in  $x_1$  that have  $\kappa(x_1) = 1/\varepsilon$  and  $\kappa(x_1) = -\frac{1}{\varepsilon+r}$ , respectively. Next we can solve for  $a$  and  $b$  using

$$a + b = x_f - x_0. \quad (6.13)$$

Combining (6.12) and (6.13) yields

$$a = \varepsilon \frac{(x_f - x_0)}{r + 2\varepsilon}, \quad b = (x_f - x_0) - \varepsilon \frac{(x_f - x_0)}{r + 2\varepsilon}. \quad (6.14)$$

## 6.5 A hypothesis

We now make the hypothesis that an optimal plant will connect the target states with a heteroclinic orbit, and that the variation in potential energy of the plant across  $[x_0, x_f]$  will be maximized. This hypothesis is based on the observations in Section 2 that when a heteroclinic orbit was introduced between the target states (via the pendulum potential), the energy cost associated with the point-to-point control decreased. Moreover, the cost continued to decrease as the change in potential energy across  $[-\pi, \pi]$  was increased. In the context of this example we will now show that a heteroclinic orbit will connect  $(x_0, 0)$  and  $(x_f, 0)$  if and only if the following constraints are satisfied:

$$0 = H(x_0) = H(x_f) = H'(x_0) = H'(x_f), \tag{6.15}$$

$$H''(x_0) > 0, \quad H''(x_f) < 0.$$

If  $0 = H(x_0) = H(x_f)$  the potential energy of the spring is the same at  $(x_0, 0)$  and  $(x_f, 0)$ , and thus the total energy is the same. Then if  $0 = H'(x_0) = H'(x_f)$ ,  $(x_0, 0)$  and  $(x_f, 0)$  will be fixed points of equal total energy. Lastly, if  $H''(x_0) > 0$  and  $H''(x_f) < 0$  then  $(x_0, 0)$  and  $(x_f, 0)$  will be saddle points. Since the plant dynamics conserve the total mechanical energy (without the influence of the control),  $(x_0, 0)$  and  $(x_f, 0)$  will be connected by a heteroclinic orbit. Conversely, suppose that any one of the conditions in (6.15) is not satisfied. Then one of the following will occur: at least one target state will not be unstable, or at least one target state will not be an equilibrium of the plant, or the target states will not be on the same level set of the conserved quantity (mechanical energy).

Now consider the follower curvature satisfying the plant optimality conditions and that connects the target states with a heteroclinic orbit:

$$\kappa(x_1) = \begin{cases} -\frac{1}{r+\varepsilon} & \forall x_1 \in \left[ x_0, \frac{x_f-x_0}{2} - \frac{\varepsilon(x_f-x_0)}{2(r+2\varepsilon)} \right) \\ \frac{1}{\varepsilon} & \forall x_1 \in \left[ \frac{x_f-x_0}{2} - \frac{\varepsilon(x_f-x_0)}{2(r+2\varepsilon)}, \frac{x_f-x_0}{2} + \frac{\varepsilon(x_f-x_0)}{2(r+2\varepsilon)} \right] \\ -\frac{1}{r+\varepsilon} & \forall x_1 \in \left( \frac{x_f-x_0}{2} + \frac{\varepsilon(x_f-x_0)}{2(r+2\varepsilon)}, x_f \right] \end{cases}$$

This is the unique plant design satisfying both the optimality conditions and the hypothesis. This is understood most easily by examining Figure 6.5 and 6.6.

Without a proof of the hypotheses, numerical methods are implemented to validate the optimality of the plant design.

## 6.6 Numerical validation of optimal plant design

When the set  $\tilde{F}$ , defined in Section 5, is considered we see that  $\kappa(x_1)$  is not necessarily continuous. There can be any number of discontinuities in  $\kappa(x_1)$  on  $[x_0, x_f]$ . To numerically validate the optimality of the design in Section 6.5 we will approximate  $\kappa(x_1)$  as having finitely many discontinuities. We will further approximate the design space by describing  $\kappa(x_1)$  in the following way:  $\kappa(x_1)$  will have  $M$  square pulses of equal length  $\frac{a}{M}$ , and there can be no overlap of the square pulses. *This finite dimensional approximation to the design space  $\tilde{F}$  will be denoted  $\tilde{F}_M$ .* An example of an admissible curvature,  $\kappa \in \tilde{F}_M$ , is shown in Figure 6.4. The location of each pulse will be described by the design variable  $y_i$ .

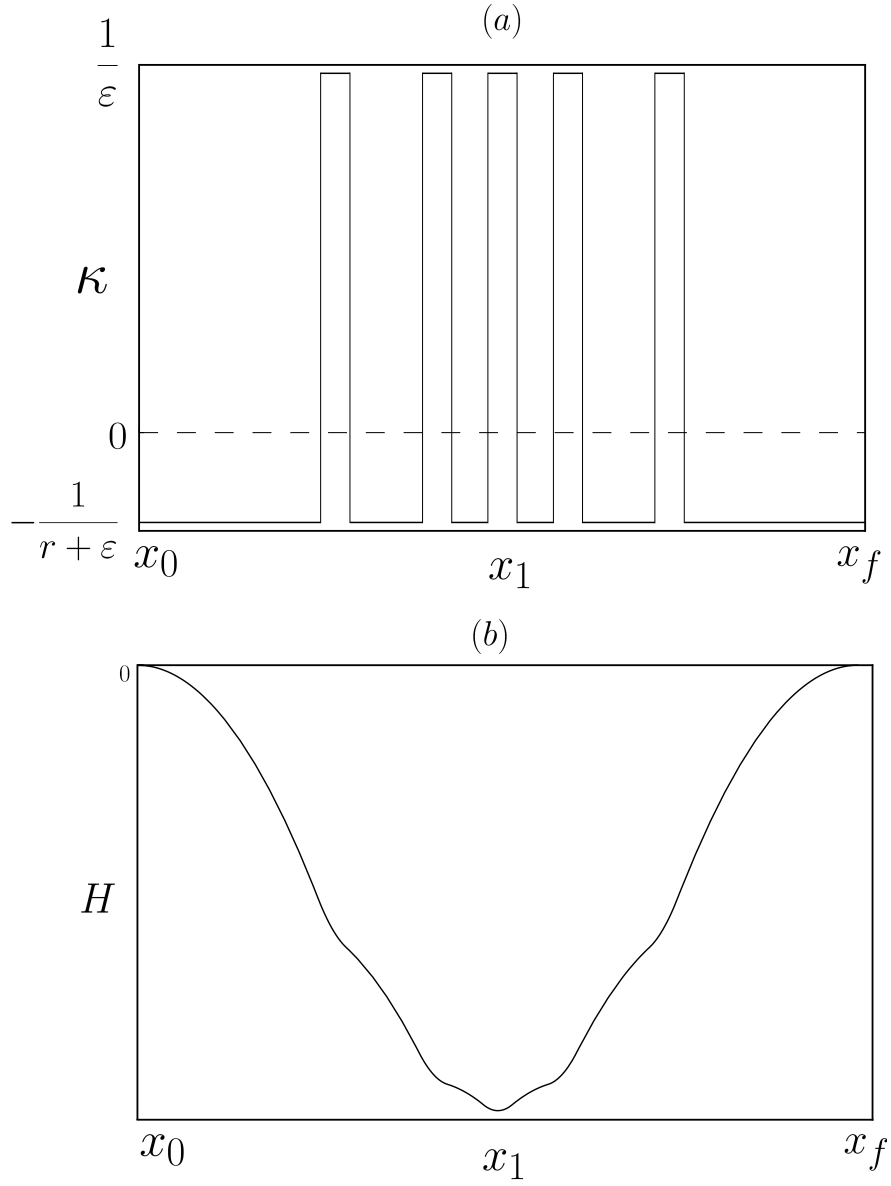


Figure 6.4: An example of  $\kappa(x)$  in the approximation to the design space where the resulting plant would be admissible and satisfy the necessary conditions given in Lemma 1 and Theorem 5.

The constraint that the pulses can have no overlap can be expressed as:

$$g_i(y) \equiv y_i - y_{i+1} + \frac{a}{M} \leq 0 \quad i = 0, 1, 2, \dots, M - 1. \quad (6.16)$$

The vector  $y$  in (6.16) is the  $M$  – tuple of values  $y_i$ . The problem has now been approximated by a finite dimensional one.

To validate the candidate plant design the following numerical experiment was conducted to check the Karush-Kuhn-Tucker (KKT) condition [11], which is an optimality condition that is frequently used in constrained optimization problems.

## 6.7 Numerical results

Table 1 shows the values chosen for the numerical experiment.

$x_0$	$x_f$	$t_0$	$t_f$	$F_0$	$\varepsilon$	$r$	<i>mass</i>	$M$
0	1	0	1.5	1	0.1	0.8	1	5

Table 1: The numerical values chosen for the optimization problem.

To compute the cost of a candidate plant design the optimal control effort for that particular plant was computed by solving (4.5) numerically using a shooting method with the Nelder-Mead simplex method to find boundary conditions for the co-state variables. Next the control effort generated by the solution is used to calculate the cost of the design according to the cost functional (3.4).

In order to check the KKT condition it is necessary to numerically compute the gradient of the cost functional with respect to the parameters of the approximated plant design space. The approach taken is to use a central difference approximation to find the derivative of the cost in the direction of each design variable. For this experiment the dimension of the approximated design space is five.

$\frac{\partial J}{\partial y_1}$	$\frac{\partial J}{\partial y_2}$	$\frac{\partial J}{\partial y_3}$	$\frac{\partial J}{\partial y_4}$	$\frac{\partial J}{\partial y_5}$
0.0650	0.0875	0.0350	0.1175	-1.0875

Table 2: Central difference approximation for the gradient of the cost functional evaluated at the candidate solution.

Clearly by the construction of this candidate solution all constraints of (6.16) are active so the KKT conditions can be expressed as

$$\begin{aligned} \frac{\partial J}{\partial y_i} + \sum_{j=1}^{M-1} \lambda_j \frac{\partial g_j}{\partial x_i} &= 0 \quad i = 1, 2, \dots, M, \\ \lambda_j &> 0 \quad j = 1, 2, \dots, M - 1. \end{aligned} \quad (6.17)$$

If we define  $G$  as

$$G = \begin{bmatrix} \frac{\partial g_1}{\partial x_1} & \frac{\partial g_2}{\partial x_1} & \dots & \frac{\partial g_{M-1}}{\partial x_1} \\ \frac{\partial g_1}{\partial x_2} & \frac{\partial g_2}{\partial x_2} & & \\ \vdots & & \ddots & \\ \frac{\partial g_1}{\partial x_M} & & & \frac{\partial g_{M-1}}{\partial x_M} \end{bmatrix}, \quad (6.18)$$

then (6.17) can be written as

$$G\lambda = \nabla J. \quad (6.19)$$

We can then solve for  $\lambda$ :

$$\lambda = (G^T G)^{-1} G^T \nabla J. \quad (6.20)$$

Combining the numerical values from table 2 into (6.20), the solution for  $\lambda$  is

$$\lambda = [0.2215 \ 0.4655 \ 0.6570 \ 0.9310].$$

Since all values of  $\lambda$  are greater than zero, the KKT conditions are satisfied. The numerical results suggest that the proposed plant design along with a control

satisfying (4.5) will indeed yield the optimal system design. Figure 6.5 plots the curvature of this design.

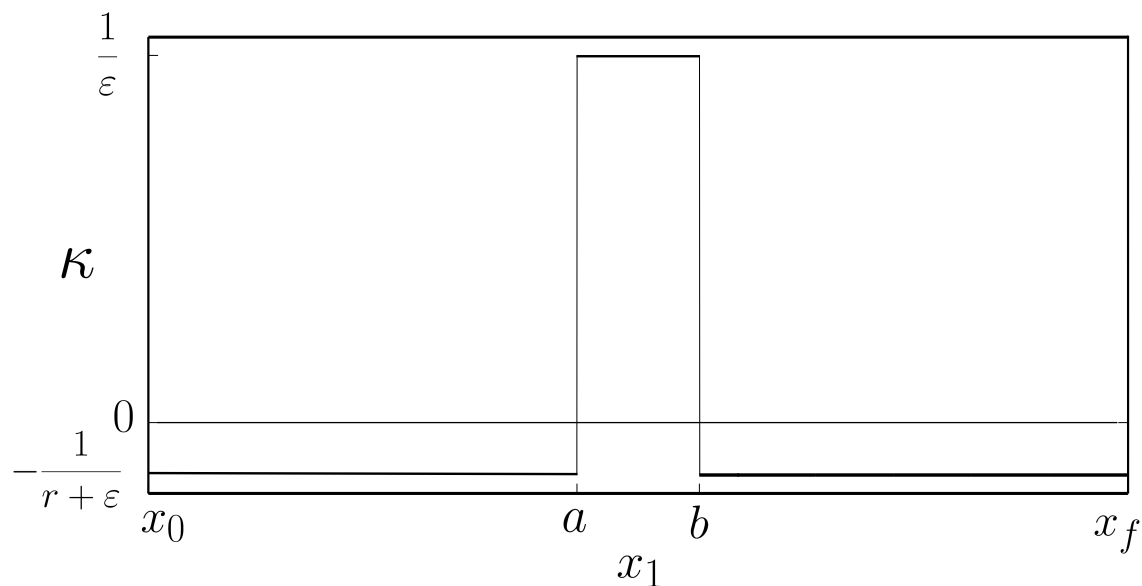


Figure 6.5: Plot of optimal cam curvature satisfying the KKT conditions.  $a$  indicates the location  $x = \frac{x_f - x_0}{2} - \frac{\varepsilon(x_f - x_0)}{2(r+2\varepsilon)}$  and  $b$  indicates the location  $x = \frac{x_f - x_0}{2} + \frac{\varepsilon(x_f - x_0)}{2(r+2\varepsilon)}$ .

The resulting cam, plotted in Figure 6.6, illustrates how the constraints described in Figure 6.3 are active throughout the cam followers path. It is clear by examining Figure 6.6 that the optimal cam design is the one which attains the greatest decrease in spring deflection between the target states while satisfying the optimality conditions. Equivalently, this is the design which maximizes the change from potential to kinetic energy during a switch.

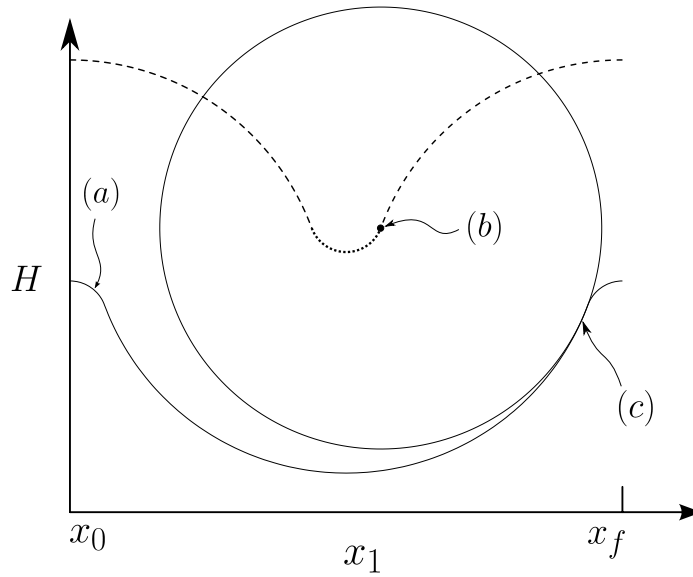


Figure 6.6: An illustration of the optimal cam follower path. The dotted and dashed line show the cam follower path at maximum and minimum curvature respectively. Arrow (a) indicates the cam profile for the corresponding cam follower path. Arrow (b) indicates the system configuration determined by the center of the cam follower, while arrow (c) indicates the contact location of the cam follower with the cam surface for the illustrated configuration.

Without any influence from the control, the state trajectories would lie on the level sets of the plant Hamiltonian. In Figure 6.7 we see how the optimal control gives rise to a trajectory makes use of the plant dynamics to execute the control objective.

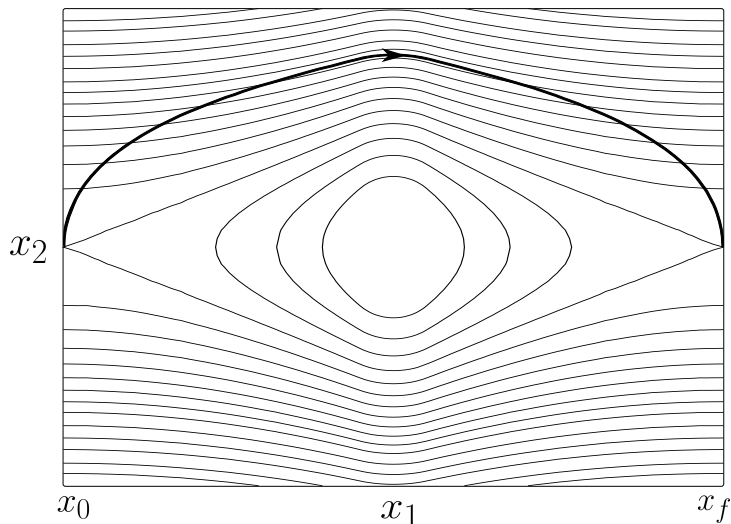


Figure 6.7: The optimal state trajectory (in bold) is plotted over the level sets of the Hamiltonian (mechanical energy) of the optimal plant design to demonstrate how the optimal trajectory tends to follow the natural motion of the plant.

## 7 Discussion and Conclusions

System optimization plays an important role in improving the performance of existing technologies. While the sequential design method can produce satisfactory system performance, it is not guaranteed to yield an optimal system design. In this thesis we considered a nested optimization strategy to simultaneously optimize the plant and control, where each was an element of an infinite dimensional space. This presented a computationally expensive optimization even with just a one degree-of-freedom system.

The primary result of this thesis was to present necessary conditions of an optimal system design to reduce the complexity of the numerical optimization.

We began by studying point-to-point control of a plant with pendulum dynamics. It was shown numerically that by increasing the natural frequency, the energy cost of actuating the system between unstable equilibria decreased. This provided the intuition that a mass can be actuated between two configurations with less energy when the two configurations are connected by a heteroclinic orbit.

Then we considered the problem of optimizing the plant and control within infinite dimensional spaces and found that a system optimality condition was that the optimal plant could not lie on the interior of the design space. This result was applied to optimize an electromechanical system with minimal numerical investigation.

While the necessary conditions presented are applicable to many simultaneous plant and controller design problems, they are limited to problems where the plant and controller are both in an infinite dimensional space. As a next step we may be able to extend these results to finite dimensional problems under some additional assumptions. Another point of further research would be to generalize the results to systems with  $n$  degrees-of-freedom, and  $m$  constraints of the form of (3.3).

## References

- [1] M. Athans and P. Falb. *Optimal Control: An Introduction to the Theory and Its Applications*. McGraw-Hill, New York, 1966.
- [2] F. Eastep, N. Khot, and R. Grandhi. Improving the active vibrational control of large space structures through structural modifications. *Acta Astronautica*, 15:383 – 389, 1987.
- [3] H. K. Fathy, J. A. Reyer, P. Y. Papalambros, and A. G. Ulsoy. On the coupling between the plant and controller optimization problems. In *Proceedings*

- of the American Control Conference, volume 3, pages 1864–1869. IEEE, June 2001.
- [4] R. V. Grandhi. Structural and control optimization of space structures. *Computers & Structures*, 31(2):139–150, 1989.
  - [5] J. Guckenheimer and P. Holmes. *Nonlinear Oscillations, Dynamical Systems, and Bifurcations of Vector Fields*, volume 42. Springer-Verlag New York, 1983.
  - [6] L. Li, J. Tao, Y. Wang, Y. Su, and M. Xiao. Effects of intake valve closing timing on gasoline engine performance and emissions. *SAE Technical Paper*, 2001-01-3564, 2001.
  - [7] John A Nelder and Roger Mead. A simplex method for function minimization. *The Computer Journal*, 7(4):308–313, 1965.
  - [8] Hajime Oniki. Comparative dynamics (sensitivity analysis) in optimal control theory. *Journal of Economic Theory*, 6(3):265–283, 1973.
  - [9] J. H. Park. Concurrent design optimization of mechanical structure and control for high speed robots. *ASME transactions on Dynamic Systems, Measurement, and Control*, 116:344–356, 1994.
  - [10] T. A. Parlikar, W. S. Chang, Y. H. Qiu, M. D. Seeman, D. J. Perreault, J. G. Kassakian, and T. A. Kiem. Design and experimental implementation of an electromagnetic engine valve drive. *IEEE Transactions on Mechatronics*, 10:482–494, 2005.
  - [11] S. S. Rao. *Engineering Optimization: Theory and Practice*. John Wiley and Sons, New Jersey, 2009.
  - [12] T. Ravichandran, D. Wang, and G. Heppler. Simultaneous plant-controller design optimization of a two-link planar manipulator. *Mechatronics*, 16:233 – 242, 2006.
  - [13] J. A. Reyer, H. K. Fathy, P. Y. Papalambros, and A. G. Ulsoy. Comparison of combined embodiment design and control optimization strategies using optimality conditions. In *ASME Design Engineering Technical Conference*. Paper DAC–21119, Pittsburgh, PA, September 2001.
  - [14] J. A. Reyer and P. Y. Papalambros. An investigation into modeling and solution strategies for optimal design and control. In *ASME Design Engineering Technical Conferences*. Paper DAC–14253, Baltimore, MD, September 2000.

- [15] Walter Rudin. *Principles of Mathematical Analysis*, volume 3. McGraw-Hill  
New York, 1964.